

HF Doppler and Ionosonde Observations on the Onset Conditions of Equatorial Spread F

B. JAYACHANDRAN,¹ N. BALAN,^{2,3} P. B. RAO,⁴ J. H. SASTRI,⁵ AND G. J. BAILEY²

The relative importance of height, vertical drift velocity, and electron density gradient of the postsunset bottomside (5.5 MHz) equatorial F region for the onset of spread F is studied using simultaneous HF Doppler radar and ionosonde observations. The study conducted for the periods January–March of 1984 and 1985 shows that the height of the F layer, determined by the time history of the prereversal enhancement of the drift velocity, is the deciding factor for the onset of equatorial spread F (ESF) with little contribution from the electron density gradient. Maximum growth rate of linear collisional Rayleigh-Taylor instability occurs at the time of peak height rather than at the time of peak velocity confirming that, for the onset of ESF, the layer should attain a threshold height. The threshold (group) height of the 5.5 MHz layer falls from ~ 450 km in 1984 (mean $F_{10.7}$ equals 120) to ~ 350 km in 1985 (mean $F_{10.7}$ equals 70); the corresponding evening peak upward drift velocities decrease from about 30 m s^{-1} in 1984 to about 20 m s^{-1} in 1985. The significant fall of the thresholds with the declining solar activity is due to the decrease in the ion-neutral collision frequency with declining solar activity; the fall of the thresholds is reflected in large decreases in the intensity and duration of the spread F .

INTRODUCTION

The most interesting physics in the equatorial F region takes place during the postsunset hours. At this time, the prereversal enhancement of the zonal electric field increases the upward $\mathbf{E} \times \mathbf{B}$ plasma drift with the effect of raising the F layer temporarily to a height where collisions are low; along with the upward drift, its fluctuations are also amplified [Balachandran *et al.*, 1992]. Beneath the F region, the E region is reduced rapidly by chemical recombination and loses its capacity to “short circuit” any irregularities that the F region might exhibit. Furthermore, the bottomside F region density gradient is increased by the loss of photoionization that earlier offset the rapid low-altitude recombination. In short, the postsunset F layer is in a state of delicate equilibrium; it is like the lifting and lowering of a system consisting of a heavy fluid resting on top of a light fluid. Any disturbance caused by background noise, neutral winds, gravity waves, or some other source can disturb the equilibrium and generate plasma irregularities [Booker, 1979; Hysell *et al.*, 1990].

If conditions (see below) are favorable, the irregularities will grow and manifest as spread F [Booker and Wells, 1938; Kelley and Hysell, 1991].

Significant advances in the understanding of the onset, growth, and maintenance of equatorial spread F (ESF) have occurred recently through a number of observational and computer simulation studies (for reviews see Fejer and Kelley [1980], Ossakow [1981], Kelley [1985], and Kelley and Hysell [1991]). ESF irregularities are known to have their onset at the bottomside of an elevated postsunset F layer [Rastogi, 1980]. On the basis of backscatter studies at Jicamarca, Farley *et al.* [1970] have suggested an altitude threshold for a particular plasma frequency level for the onset of ESF. Further studies on the association between the ESF and the height of the F layer using various other techniques have revealed that the threshold height for the onset of ESF depends on the postsunset F region vertical drift velocity, season, and solar activity [Tsunoda, 1981; Sastri, 1984; Jayachandran *et al.*, 1987]. However, on the basis of ionosonde data, Abdu *et al.* [1982] have shown that bottomside electron density scale height and ion-neutral collision frequency near the base of the F layer determine the postsunset onset of ESF.

Theoretical advances have covered a wide area involving both linear and nonlinear analysis as well as computer simulation studies of various plasma instability processes (for reviews, see the works by Ossakow [1981] and Kelley [1985]). On the basis of numerical simulation of the collisional Rayleigh-Taylor (RT) instability mechanism, Scannapieco and Ossakow [1976] have shown, for the first time, that under favorable conditions (high altitude of the F peak and/or steep bottomside electron density gradient) the instability (similar to the hydrodynamic instability associated with a heavy

¹Department of Physics, University of Kerala, Trivandrum, India.

²Department of Applied and Computational Mathematics, University of Sheffield, Sheffield, England.

³On leave from the University of Kerala, Trivandrum, India.

⁴National MST Radar Center, Tirupati, India.

⁵Indian Institute of Astrophysics, Bangalore, India.

Copyright 1993 by the American Geophysical Union.

Paper number 93JA00302.

0148-0227/93/93JA-00302\$05.00

fluid resting on top of a light fluid) causes linear growth of irregularities in the bottomside *F* region, which, in turn, cause plasma density depletions or plasma bubbles. The bubbles then rise nonlinearly to the topside by the enhanced $\mathbf{E} \times \mathbf{B}$ drift. The bubble development is in accord with many observations [Woodman and La Hoz, 1976; Aggson *et al.*, 1992].

The above experimental and theoretical studies show that the altitude of the *F* layer, prereversal drift velocity, and bottomside electron density gradient are the important parameters which determine the conditions for ESF onset. However, the relative importance of these parameters in the generation and maintenance of ESF has not yet been examined in detail. It is in this context the present study is undertaken. The study uses simultaneous HF Doppler radar and ionosonde observations conducted at two nearby equatorial stations Trivandrum (dip 0.5° N) and Kodaikanal (dip 3.5° N) during the declining solar activity periods January–April 1984 and 1985. During these two periods the mean solar flux index *F*10.7 is about 120 and 70, respectively.

OBSERVATIONS AND ANALYSIS

The HF Doppler technique used for the vertical plasma drift velocity measurements at Trivandrum (8.5° N, 77° E; dip 0.5° N) has been described in detail by

Balan et al. [1982]. For the present study, to probe plasma drifts in the postsunset bottomside *F* region, the system was operated at a frequency of 5.5 MHz with a pulse width of $100 \mu\text{s}$ and a pulse repetition frequency of 50 Hz. The vertically reflected ionospheric signal was received by a phase coherent receiver which provided sampled quadrature outputs of $A \cos \phi$ and $A \sin \phi$, where *A* and ϕ are the amplitude and phase of the received signal, respectively. The quadrature signals were recorded on a chart recorder operated at a speed of 10 cm min^{-1} . While recording the Doppler signal the gate delay (set to a resolution of $10 \mu\text{s}$ at the peak of the received signal) was also noted. The observations were made during January–April 1984 and 1985 from 1700 local standard time (LST) to the time when the critical frequency fell below the operating frequency of 5.5 MHz, which generally occurred between midnight and 0200 LST. However, the observations beyond midnight are not considered in the present study as the primary aim of the study is to investigate the onset conditions of spread *F* which begins well before midnight.

The Doppler data (for samples, see Figure 1) are analyzed at 5-min time intervals using 1-min samples. The number of both positive and negative peaks of the quasi-sinusoidal variations of the quadrature channels are counted for the sampling period of 1 min; the four values thus obtained are averaged to get the Doppler

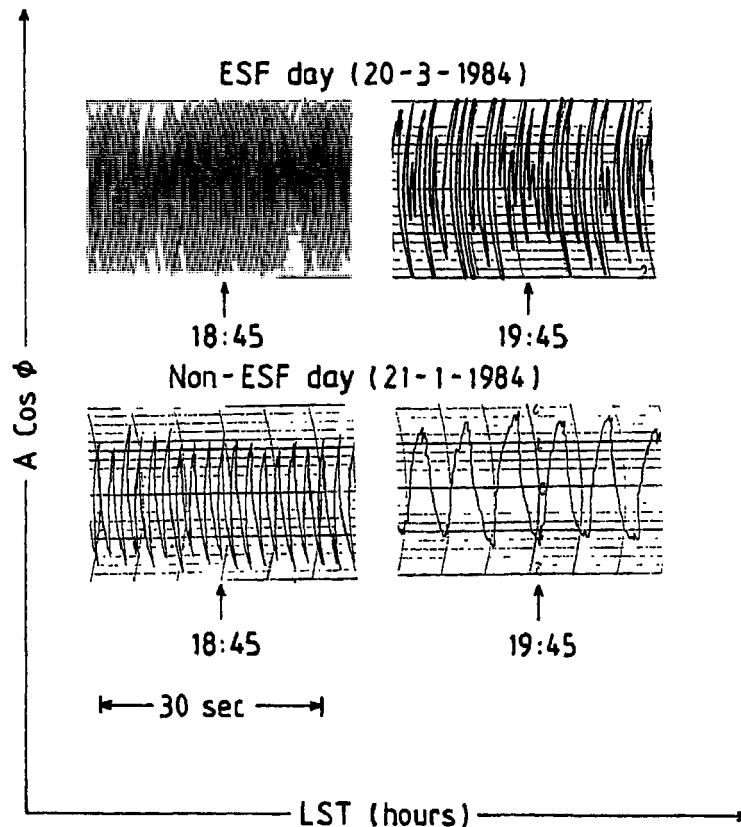


Fig. 1. Sample Doppler records from the quadrature channel $A \cos \phi$ during (1845 LST) and after (1945 LST) the prereversal enhancement of vertical drift velocity on a typical spread *F* (March 20, 1984) and non-spread *F* (January 21, 1984) day. LST is the local standard time at longitude 82.5° E.

count (number of cycles per minute), which is then converted to the drift velocity V_z using the expression $V_z = \lambda \Delta F / 2$, where ΔF is the Doppler frequency (number of cycles per second) and λ is the operating wavelength. In analyzing the Doppler data under the normal conditions of no spread F there may be an error of one cycle per minute in the Doppler count. This corresponds to an uncertainty of about 0.5 m s^{-1} . Under spread F conditions, since the quasi-sinusoidal variations do not have equal size (see Figure 1), the variations that exceed 50% of the maximum size are counted. This procedure gives an estimated uncertainty of 2–3 m s^{-1} in the derived drift velocity. The group height h' is obtained from the time delay of the gate pulse. Under normal conditions of no spread F , h' has an uncertainty of 1.5 km (determined by the resolution of the gate pulse, 10 μs). Under spread F conditions, because the signal undergoes Doppler broadening, the uncertainty in h' increases to an estimated maximum of about 20 km during strong spread F . It should be noted that the measured group height (h') during the early postsunset hours 1700–2100 LST, important for ESF onset, would only be slightly above the corresponding true height (h) since $f_0 F_2$ during this period is likely to be well above the operating frequency. For more details of the analysis of the Doppler data and the uncertainties associated with the derived results, see the works by *Balan et al.* [1982, 1992].

The derived drift velocity is to be regarded, in the strict sense, as apparent as it includes a contribution from the decay of the layer. This contribution, however, is negligible during the period relevant for ESF onset (1700–2100 LST) and is present to almost the same extent on both ESF and non-ESF days. During the postsunset period the contribution from the decay of the layer is negligible (< 5%) provided the reflecting layer is above about 300 km altitude [*Bittencourt and Abdu*, 1981]. For the postsunset periods of the days under investigation the reflection height remained above 300 km altitude during the period most important for ESF onset (1700–2100 LST). Thus the measured drift velocities can be considered as true drift velocities during this period. In fact, the drift velocities measured by the HF Doppler radar at Trivandrum, and the incoherent scatter radar at Jicamarca are in very good agreement during the period 1700–2100 LT [*Fejer et al.*, 1979; *Balan et al.*, 1992].

The operation of a C_4 ionosonde at Kodaikanal (10.2° N, 77.5° E; dip 3.5° N) during the same period as the Doppler observations provided good quality ionograms at 15-min intervals for 18 common days (9 ESF days and 9 non-ESF days) in both 1984 and 1985. The ionograms are reduced to N - h profiles using a true height analysis program. From the N - h profiles the electron density gradient (dN_e/dh , the electron density difference in a height interval of 20 km centered at the 5.5 MHz plasma frequency level) is computed at 15-min intervals for the period relevant to the ESF onset (1700–2100

LST). The postsunset spread F at Kodaikanal is generally of range type; for typical examples of the ionograms, see the works by *Sastri and Murthy* [1975].

The generation of bottomside equatorial spread F irregularities is thought to be due to a Rayleigh-Taylor (RT) instability mechanism [*Ossakow et al.*, 1979; *Kelley*, 1985]. In order to examine if the ESF onsets studied in this paper are in accordance with this instability mechanism, the growth rate of the instability is computed at 15-min time intervals for all the ESF and non-ESF days under consideration. The growth rate (γ) is computed using the following expression [*Ossakow et al.*, 1979]:

$$\gamma = \frac{1}{H} \left(\frac{g}{\nu_{in}} + V_z \right) - \beta \quad (1)$$

The above growth rate is linear, local, and nondissipative and therefore has no wave number dependence; it is a good approximation for an intermediate scale mode. In the above expression the first term on the right-hand side gives the RT instability growth rate, the second term gives the cross-field instability growth rate, and the third term gives the recombination rate; H is the electron density scale height, g is the acceleration due to gravity, and ν_{in} is the ion-neutral collision frequency. The electron density scale height, $H = [N_e^{-1} dN_e/dh]^{-1}$, of the 5.5 MHz reflection layer, whose vertical drift velocity (V_z) has been measured by the HF Doppler radar, is determined from the N - h profiles and values for the parameters ν_{in} and β (recombination rate) are calculated from the following expressions [*Strobel and McElroy*, 1970]:

$$\nu_{in} = 2.4 \times 10^{-11} T^{1/2} N_n \quad (2)$$

$$\beta = K_1 n(O_2) + K_2 n(N_2) \quad (3)$$

where K_1 and K_2 are temperature-dependent reaction rates [*McFarland et al.*, 1973], and N_n , $n(O_2)$, and $n(N_2)$ are the number densities of neutral air, molecular oxygen, and molecular nitrogen, respectively. The number densities N_n , $n(O_2)$, and $n(N_2)$ and the neutral temperature T are obtained from CIRA (1972).

It should be noted that the values of N_e and dN_e/dh (hence γ) cannot be determined to any degree of accuracy under spread F conditions. The inaccuracies, however, do not affect the main objective of the study which, as stated above, is to investigate the relative importance of h' , V_z , and dN_e/dh to the linear growth rate of the instability leading up to the onset of spread F . However, the variations of dN_e/dh and γ , shown in Figures 2, 3, and 4, extend beyond the time of onset of spread F . These extensions are shown for the sake of completeness and are marked differently to distinguish them from the parts of the variations that are important in the main theme of the study. It should also be noted that the HF Doppler radar operates at a single

frequency of 5.5 MHz, which, in general, corresponds to a level where the electron density (N_e) varies steeply in the postsunset bottomside *F* region. For a study of the relative importance of h' , V_z , and dN_e/dh it is considered appropriate to evaluate dN_e/dh at the same plasma frequency level where h' and V_z are measured by the radar.

RESULTS AND DISCUSSION

Figure 1 shows sample Doppler records during and after the prereversal enhancement of the vertical drift velocity on typical ESF (March 20, 1984) and non-ESF (January 21, 1984) days. The samples illustrate that the Doppler frequency which has been monochromatic during the prereversal enhancement period changes to a broadened spectrum (showing the presence of spread *F*) after the enhancement on the ESF day, while on the non-ESF day it remains monochromatic throughout. Also, the Doppler frequency and hence the vertical drift velocity are both greater on the ESF day than on the non-ESF day. The sample Doppler data shown for 1845 and 1945 LST correspond to vertical drift velocities of 45 and 12 m s⁻¹, respectively, on the ESF day and 14 and 3 m s⁻¹, respectively, on the non-ESF day.

The local time variations of the vertical drift velocity (V_z), the group height (h'), the electron density gradient (dN_e/dh), and the instability growth rate (γ)

for the above typical ESF and non-ESF days (Figure 1) are shown in Figure 2. Before about 1800 LST the drift velocities are nearly equal on both days. After this time on March 20, 1984, the drift velocity undergoes a sharp prereversal enhancement with a peak velocity of 55 m s⁻¹ at 1900 LST and a downward reversal at 1955 LST; the layer is raised to a group height of 540 km. On this day, strong spread *F* is observed with onset at 1940 LST when the layer is at a group height of about 450 km. Duration of the spread *F* is indicated by the horizontal strip in Figure 2; spread *F* disappears when the layer descends to a group height of about 275 km. However, on January 21, 1984, the prereversal enhancement of the drift velocity is weak and the layer is not raised. Spread *F* is not observed on this day. There is little difference in the electron density gradients on the 2 days until about 1900 LST. After this time, contrary to expectation, the electron density gradient on the ESF day is lower than that on the non-ESF day; this is because the layer is located at a greater height on the ESF day than on the non-ESF day. The instability growth rate (γ) increases from about 1830 LST and reaches a maximum near the time of spread *F* onset on the spread *F* day; the growth rate does not increase on the non-spread *F* day.

Some noted features of the drift velocity variations (Figure 2) on the ESF and non-ESF days are (1) the

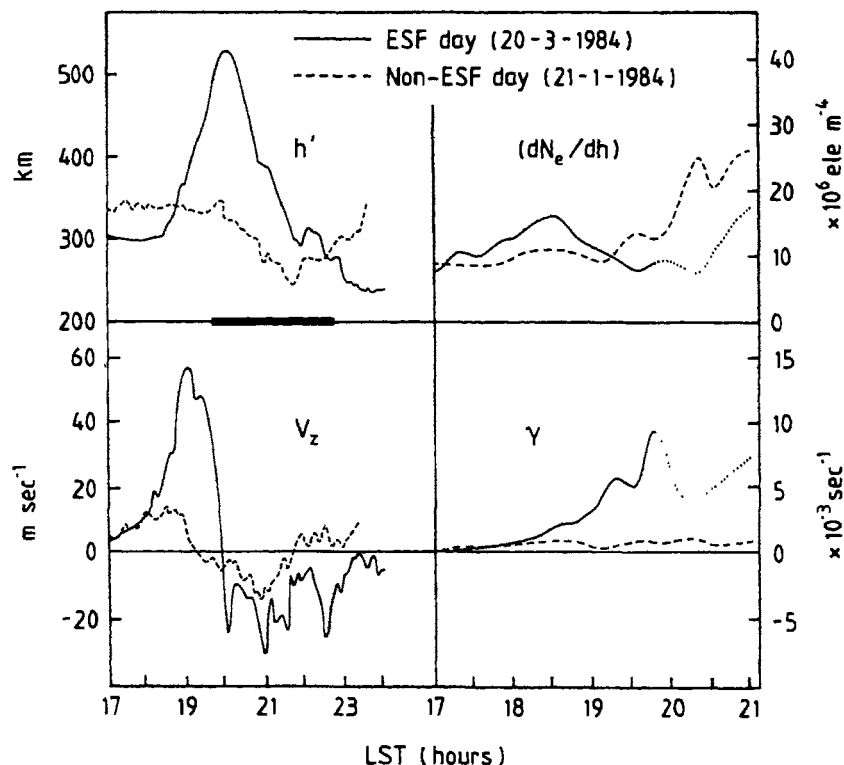


Fig. 2. Time variations of the group height (h'), vertical drift velocity (V_z), bottomside electron density gradient (dN_e/dh), and RT instability growth rate (γ) on the typical spread *F* (solid curves) and non-spread *F* (dashed curves) days noted in Figure 1. The solid horizontal bar denotes the duration of spread *F*. The values of dN_e/dh and γ (marked by dots) during the spread *F* period have large uncertainties (see text).

drift reversal occurs about 40 min later on the ESF day than on the non-ESF day and (2) the fluctuations of the drift velocity are stronger on the ESF day than on the non-ESF day. The fluctuations on the ESF day have a quasi-period of about 1 hour and an amplitude of about 20 m s^{-1} . Recently, *Balachandran et al.* [1992] have shown that along with the vertical drift velocity its fluctuations are also amplified during the postsunset period, and the fluctuations attain maximum amplitude at around the time of downward reversal, the general time of onset of ESF; the characteristics of the fluctuations suggest that they are of gravity wave origin. When the drift velocity (and layer height) corresponding to a fixed electron density level fluctuates (because of fluctuating electric fields), it implies that, at the corresponding mean height, the electron density itself is fluctuating. As the layer rises, the electron density fluctuations are amplified, as indicated by the amplification of the vertical drift velocity fluctuations, and can trigger the onset of spread *F* when the layer reaches the altitude favorable for ESF occurrence. It should be noted that the fluctuations in V_z are unlikely to be the manifestation of the instability underway because strong fluctuations exist well before the onset of spread *F* (see also the works by *Jayachandran et al.* [1987] and *Balan et al.* [1992]). *Somayajulu et al.* [1991] have reported

from an analysis of equatorial ionograms that fluctuating vertical plasma drifts, or equivalently fluctuating east-west electric fields, are conducive to the occurrence of ESF throughout the night. The features 1 and 2 are found to be true for all the ESF and non-ESF days under investigation. However, feature 2 does not occur in the mean drift velocity variations (see Figures 3 and 4).

The local time variations of mean V_z , h' , dN_e/dh and γ for the ESF and non-ESF days in 1984 are shown in Figure 3. The vertical bars denote the standard deviations. The mean prereversal peak drift velocity and group height are about 45 m s^{-1} and 470 km, respectively, for the ESF days and about 20 m s^{-1} and 385 km for the non-ESF days. Mean ESF onset (at 1940 LST) is close to the time of mean peak height, which is about 40 min past the time of mean peak velocity. Spread *F* is found to be generally strong with mean duration of about 3.5 hours (see the horizontal strip in Figure 3). Mean ESF ceases when the layer descends to a mean group height of about 260 km. As in the case of the typical ESF and non-ESF days, the mean electron density gradient is little different for the ESF and non-ESF days until about 1900 LST. After this time, contrary to expectation, the electron density gradient is lower for the ESF days than for the non-ESF days. This is as it should be, because the layer

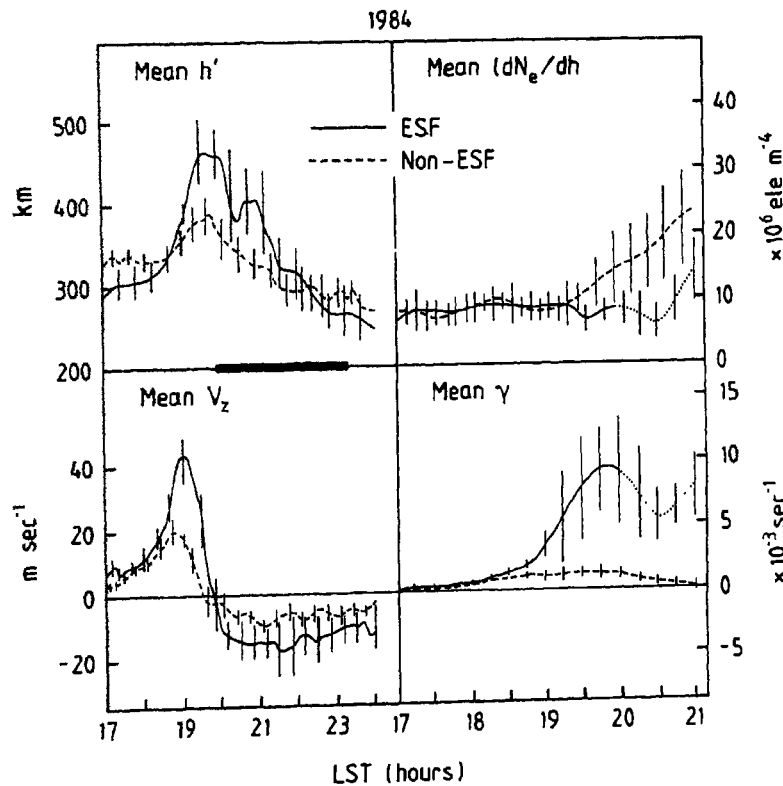


Fig. 3. Time variations of mean group height (h'), mean vertical drift velocity (V_z), mean electron density gradient (dN_e/dh), and mean RT instability growth rate (γ) for the spread *F* (solid curves) and non-spread *F* (dashed curves) days in 1984. The vertical bars are standard deviations from the mean values. The solid horizontal bar denotes the average duration of spread *F*. The values of dN_e/dh and γ (marked by dots) during the spread *F* period have large uncertainties (see text).

is located at greater heights on the ESF days than on the non-ESF days. The mean growth rate (γ) of the instabilities for the ESF days increases when the layer starts to drift rapidly upward and reaches a maximum when the layer is at its peak altitude; the maximum growth rate (10^{-2} s^{-1}) is about 10 times its value before the growth rate begins to increase. The growth rate remains low (at about 10^{-3} s^{-1}) throughout the postsunset period for the non-ESF days.

Figure 4 is similar to Figure 3 but for 1985. In 1985, the mean prereversal peak drift velocity and group height are about 20 m s^{-1} and 400 km , respectively, for the ESF days and about 12 m s^{-1} and 300 km for the non-ESF days. The mean drift velocity reverses significantly later (about 40 min) on the ESF days than on the non-ESF days. Mean ESF onset occurs at 2030 LST (when the layer is at its mean peak altitude); this time is about 1.5 hours past the time of mean peak velocity. Spread *F* is found to be generally weak with a mean duration of about 1 hour (denoted by the thick horizontal bar in Figure 4). Mean ESF ceases when the layer descends to a mean group height of about 325 km . The mean values of the electron density gradient are slightly higher for the non-ESF days. The variations of mean γ remain the same for the ESF and non-ESF days until about 1845 LST; beyond this time, γ increases to a maximum value of about $5 \times 10^{-3} \text{ s}^{-1}$ for the ESF days and shows a decreasing trend for the non-ESF days.

Comparison of Figures 3 and 4 highlights the following points: (1) mean ESF onset occurs at the time of peak height rather than at the time of peak velocity (an observation consistent with that of *Farley et*

al. [1970]) in both 1984 and 1985; (2) evening downward reversal occurs later on the ESF days than on the non-ESF days (by about 15 min in 1984 and 40 min in 1985); (3) in 1984, when the postsunset drift velocity is high, the peak height is attained in about 45 min after the time of peak velocity; and (4) in 1985, when the postsunset drift velocity is low, the drift velocity has to be maintained upward for a longer time (about 1.5 hours after the time of peak velocity) for the layer to attain an altitude favorable for ESF onset. These observations confirm the importance of the time history of the prereversal enhancement of the drift velocity for ESF occurrence. In a previous study, *Sastri* [1984] has shown that the onset and duration of ESF bears a direct relation to the postsunset time history of the *F* region vertical drifts and hence the altitude attained by the *F* layer. It may be noted here that the evening reversal of the zonal plasma drift is also delayed on spread *F* days compared to that of non-spread *F* days [*Vyas and Chandra*, 1991].

Figures 2–4 illustrate that (1) the peak altitude attained by the *F* layer depends on the time history of the prereversal enhancement of the vertical drift velocity, (2) once the layer crosses a threshold altitude conditions are set for the growth of RT instability which ultimately leads to the onset of ESF, and (3) the magnitude of the bottomside electron density gradient does not seem to play a role for the onset of ESF. The importance of the height and velocity of the postsunset *F* layer for the onset of ESF is illustrated further in Figures 5*a* and 5*b*, which show the peak group height ($h' \text{ max}$) and peak velocity ($V_z \text{ max}$) attained by the

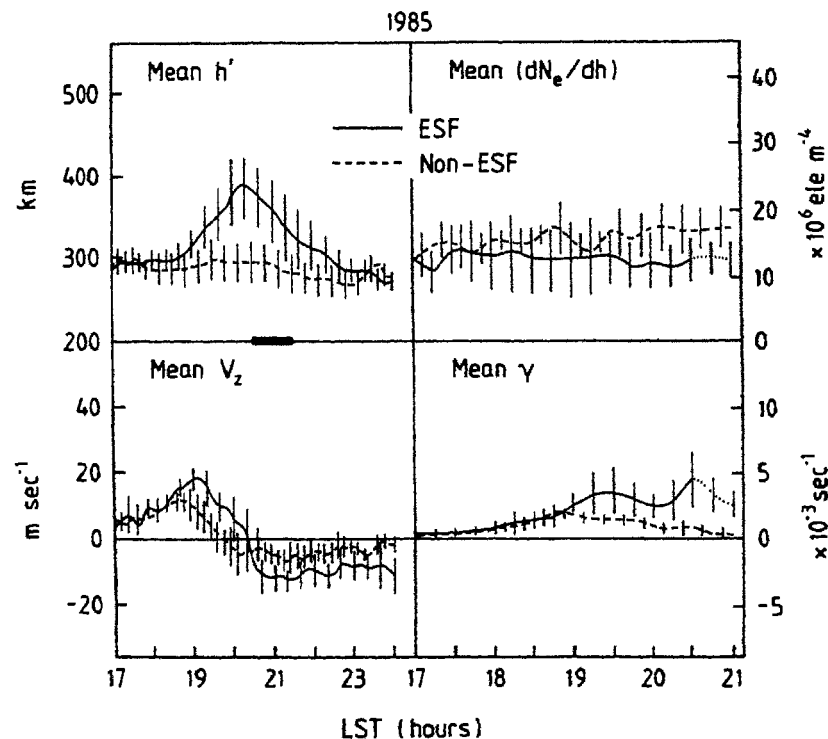


Fig. 4. Same as Figure 3 but for 1985.

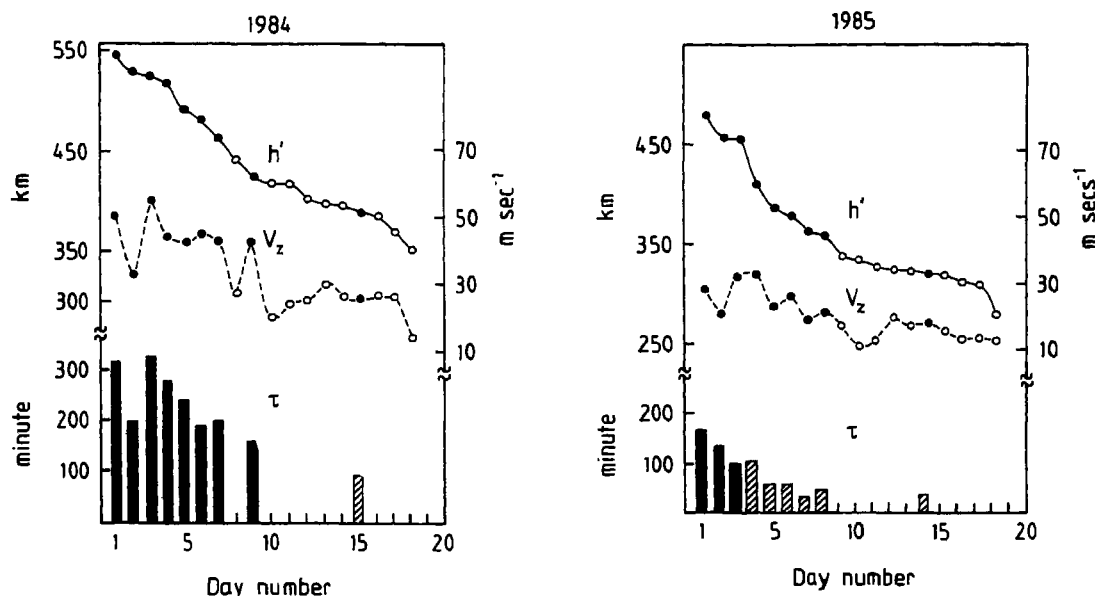


Fig. 5a. Maximum group height (h' max) and vertical drift velocity (V_z max) attained by the 5.5 MHz layer on individual spread F (solid circle) and non-spread F (open circle) days in 1984. The days are arranged in the order of decreasing height. The vertical bars (lower panel) denote the duration of spread F (τ); solid and dashed vertical bars correspond to strong and weak spread F , respectively.

Fig. 5b. Same as Figure 5a but for 1985.

5.5 MHz layer on different days of observations in 1984 and 1985, respectively. The days of observation are arranged in the order of decreasing height. Closed circles correspond to ESF days and open circles to non-ESF days. Vertical bars give the duration of ESF; solid and dashed vertical bars indicate whether the ESF was strong or weak, respectively. (The nature of the ESF is decided from the spread of the ionospheric returns as seen in the visual display of the HF Doppler radar, the Doppler records and the ionograms.) It is clear from Figure 5a that in 1984, ESF occurred invariably when the group height and vertical drift velocity were greater than 450 km and 30 $m\ s^{-1}$, respectively; in 1985 (Figure 5b) these limits were reduced to about 350 km and 20 $m\ s^{-1}$, respectively. Spread F events were generally strong and long-lived (with an average duration of about 3.5 hours) in 1984 compared to the weak short-lived events (with an average duration of about an hour) in 1985 (see the vertical bars in Figures 5a and 5b). The intensity and duration of spread F in the 2 years were in accordance with the corresponding mean peak values of h' and V_z . No spread F occurred when the height and velocity were below 300 km and 15 $m\ s^{-1}$, respectively. Figures 5a and 5b also illustrate the importance of the time history of the prereversal enhancement of the drift velocity; a comparatively low velocity maintained upward for a longer time raises the layer to nearly the same altitude as a high velocity maintained upward for a shorter time.

The importance of h' , V_z , and H for the onset of postsunset equatorial spread F has been studied by several investigators. For example, using ionosonde data, *Abdu et al.* [1982] have shown that the generation of

spread F irregularities in the Brazilian equatorial station Fortaleza depends on the bottomside F region values of h' and H . Though the relative importance of the two parameters is not evident in this study, it appears that h' is more important than H . This relative importance is shown by *Abdu et al.* [1983] in a later paper which puts threshold values for h' and V_z as necessary conditions for the occurrence of spread F . The peculiarity of the Brazilian longitude, i.e., having the largest magnetic declination (about 22°W), is also shown to control the prevreversal enhancement of V_z and the occurrence of spread F [*Abdu et al.*, 1992], see also the works by *Tsunoda* [1985]. It should be noted that the magnetic declination of Trivandrum is small (about 2°W). *Scannapieco and Ossakow* [1976] and *Ossakow et al.* [1979], through numerical simulation studies, have also shown that varying the altitude of the F region peak for fixed H has more pronounced effect in the linear and nonlinear evolution of the collisional RT instability than varying H for fixed F region altitude. The above studies demonstrate that the postsunset rise of the F layer is more important than the bottomside electron density scale height for the onset of spread F . Recently, *Mendillo et al.* [1992], using multi-diagnostic observations and semiempirical modeling, have shown that the postsunset rise of the F region and the availability of a seed perturbation to launch the RT mechanism (together with a weak transequatorial thermospheric wind) are the requirements for RT instability growth leading to the onset of equatorial spread F .

In the present study, by using simultaneously measured values of h' , V_z , and H corresponding to a fixed plasma frequency level of the postsunset bottomside F

region, it is shown that height and vertical drift velocity are the deciding factors for the growth of the irregularities leading to the onset of spread *F* with little contribution from electron density scale height; the fluctuations in the drift velocity, caused by internal gravity waves and amplified during the prereversal enhancement period [Balachandran *et al.*, 1992], can act as the seed for the initial perturbation. Electron density scale height may have a role to play in the growth of the irregularities when the layer does not attain the threshold height. The results showing that the maximum growth rate occurring at the time of peak height (when the velocity is almost zero) rather than at the time of the peak drift velocity, suggest that the gravitational-collisional drift term (g/ν_{in}) is more important than the cross-field term (V_z) for the instability growth rate. Thus the ion-neutral collision frequency ν_{in} and the recombination coefficient β , which are height dependent, are the main governing parameters for the plasma instability growth rate and hence the onset of ESF. Therefore, for the onset of ESF it is essential that the layer attains a threshold height which is determined by the time history of the prereversal enhancement of the vertical drift velocity.

However, comparing Figures 3 and 4 (and also Figures 5a and 5b), it can be seen that for nearly equal values of h' (peak value about 400 km) and V_z (peak value about 20 m s⁻¹) in 1984 and 1985, the irregularity growth rate (γ) increases and leads to the onset of spread *F* in 1985, while it does not increase in 1984. This difference in the growth rate of the irregularities with declining solar activity is due to the decrease in the ion-neutral collision frequency ν_{in} as illustrated in Figure 6. This figure shows the altitude variation of ν_{in} at 2000 LST for day 80 in 1984 (dashed curve) and day 75 in 1985 (solid curve). The days are magnetically quiet and have values of $F10.7$ equal to 122 and 70, respectively. The values of ν_{in} are computed using equation 2 of this paper and the MSIS 86 (mass spectrometer/incoherent scatter 86) atmospheric model [Hedin,

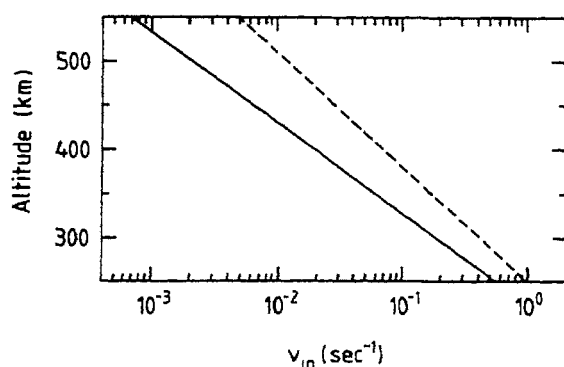


Fig. 6. Altitude variations of ion-neutral collision frequency (ν_{in}) at 2000 LST on day 80 in 1984 (dashed curve) and on day 75 in 1985 (solid curve). The values of $F10.7$ on these days are 122 and 70, respectively.

1987]. As seen in Figure 6, the values of ν_{in} in 1985 are much less than those in 1984 at all altitudes. For example, at 400 km (the peak altitude of the 5.5 MHz layer at which spread *F* occurred in 1985 and did not occur in 1984), ν_{in} in 1985 ($1.8 \times 10^{-2} \text{ s}^{-1}$) is about 4 times less than that in 1984 ($6.6 \times 10^{-2} \text{ s}^{-1}$). The variations of ν_{in} for other local times are found to be similar to those shown in Figure 6; however, the difference in ν_{in} between 1984 and 1985 is slightly larger for earlier local times and smaller for later local times. The values of the recombination rate β computed using the MSIS-86 atmospheric model are also found to be much less (about 7 times) in 1985 than in 1984. However, the contribution of β to the growth rate γ is negligible because γ is of the order of $10^{-3} - 10^{-2} \text{ s}^{-1}$ (see Figures 2, 3, and 4), while β is found to vary from about 10^{-4} (at 250 km) to about 10^{-9} s^{-1} (at 550 km). Thus the fall in the threshold height for the onset of spread *F* from 1984 to 1985 observed in the present study is due to the decrease of the ion-neutral collision frequency with declining solar activity.

The evening *F* layer is raised by the eastward dynamo electric field caused by *F* region neutral winds [Rishbeth, 1971; Heelis *et al.*, 1974]. This elevation of the *F* layer causes the mean ion-neutral collision frequency (and hence the integrated Pedersen conductivity) in a given magnetic tube of the *F* region plasma to decrease. It has been shown that the same eastward electric field that raises the *F* layer can also appreciably decrease the Pedersen conductivity in the *E* region [Hanson *et al.*, 1983]. Both these effects will contribute to the destabilization of the *F* layer and hence enhance the onset conditions of spread *F*.

To examine the growth rates of the RT instability for the spread *F* and non-spread *F* events studied in this paper, a simplified linear theory is used. The results of the study which has used local values of the ionospheric parameters illustrate that the generation and growth of the irregularities leading to the onset of spread *F* are possible under local ionospheric conditions; local values of the parameters could be different from their field line integrated values. Hanson *et al.* [1986] have shown that the simplified approach of considering only the equatorial values of the relevant parameters compares favorably well with the calculations made taking into account the field line integrated values. However, Anderson and Haerendel [1979], who have used field line integrated values of the ionospheric parameters, have found significant differences in the growth rate of the irregularities. Experimentally, it is difficult to assess the importance of the field line integrated values of the parameters. It may be that once the irregularities (or bubbles) are generated locally the subsequent growth and vertical ascension of the bubbles could be determined by the field line integrated values of the ionospheric parameters and the ambient east-west electric field [Anderson and Haerendel, 1979; Cakir *et al.*, 1992].

In recent years, the effect of neutral air winds on the growth rates of spread *F* irregularities has been considered [Kelley, 1985; Raghavarao et al., 1987; Maruyama, 1988]. Horizontal winds are known to induce significant instability in the *E* region [Chiu and Straus, 1979]. However, Kelley [1985] has shown that horizontal winds in the presence of a tilted ionosphere can also destabilize the bottomside *F* layer. Vertical (downward) winds are also known to have significant positive effect on the instability growth in the *F* region [Raghavarao et al., 1987]. It is to be noted that the neutral air wind effects on the instability growth rates are not included in the present investigation. The occurrence of ESF at lower heights and velocities on the 2 days considered in this investigation (day numbered 15 in Figure 5a and 14 in Figure 5b) could be due to the instability induced by neutral air winds. Recently, Mendillo et al. [1992] have suggested that the absence of spread *F* on a night during a spread *F* season is due to the suppression of instability growth rates by a transequatorial neutral wind.

CONCLUSIONS

The relative importance of height, vertical drift velocity, and electron density gradient of the postsunset bottomside (5.5 MHz) equatorial *F* region for the onset of spread *F* is studied using simultaneous HF Doppler radar and ionosonde observations. The study conducted for the periods January–March of 1984 and 1985 shows that (1) the height and drift velocity are the deciding factors for the onset of equatorial spread *F* (ESF) with little contribution from the electron density gradient; (2) the importance of the drift velocity (both magnitude and duration of the prereversal enhancement) is to raise the layer to altitudes where ion-neutral collisions are low; (3) fluctuations in the drift velocity, caused by internal gravity waves and amplified during the prereversal enhancement period [Balachandran et al., 1992], can act as the seed for the generation of the initial perturbation; (4) maximum growth rate of linear collisional Rayleigh–Taylor instability occurs at the time of peak height (when the velocity is almost zero) rather than at the time of peak velocity confirming that, for the onset of ESF, the layer should attain a threshold height; (5) the threshold (group) height of the 5.5 MHz layer falls from about 450 km in 1984 (mean *F*_{10.7} equals 120) to about 350 km in 1985 (mean *F*_{10.7} equals 70) (the corresponding evening peak upward drift velocities decrease from about 30 m s⁻¹ in 1984 to about 20 m s⁻¹ in 1985); (6) the significant fall of the thresholds with declining solar activity is due to the decrease in the ion-neutral collision frequency with declining solar activity; and (7) the fall of the thresholds are reflected in large decreases in the intensity and duration of the spread *F*.

Acknowledgments. The HF Doppler radar was developed [Balan et al., 1982] and operated with support from

ISRO RESPOND (India) programme. One of the authors (B.J) would like to thank UGC (India) for the award of a Teacher Fellowship under FIP. This work was also supported by the Science and Engineering Research Council (UK) under grant GR/G 05087.

The Editor thanks D.L. Hysell and another referee for their assistance in evaluating this paper.

REFERENCES

- Abdu, M. A., R. T. De Medeiros, and J. H. A. Sobral, Equatorial spread *F* instability conditions as determined from ionograms, *Geophys. Res. Lett.*, **9**, 692, 1982.
- Abdu, M. A., R. T. De Medeiros, J. A. Bittencourt, and I. S. Batista, Vertical ionization drift velocity and range type spread *F* in the evening equatorial ionosphere, *J. Geophys. Res.*, **88**, 399, 1983.
- Abdu, M. A., I. S. Batista, and J. H. A. Sobral, A new aspect of magnetic declination control of equatorial spread *F* and *F* region dynamo, *J. Geophys. Res.*, **97**, 14897, 1992.
- Anderson, D. N., and G. Haerendel, The motion of depleted plasma regions in the equatorial ionosphere, *J. Geophys. Res.*, **84**, 4251, 1979.
- Aggson, T. L., N. C. Maynard, W. B. Hanson, and J. L. Saba, Electric field observations of equatorial bubbles, *J. Geophys. Res.*, **97**, 2997, 1992.
- Balachandran Nair, R., N. Balan, G. J. Bailey, and P. B. Rao, Spectra of the ac electric fields in the postsunset *F* region at the magnetic equator, *Planet. Space Sci.*, **40**, 655, 1992.
- Balan, N., B. V. Krishna Murthy, C. Raghava Reddy, P. B. Rao, and K. S. V. Subbarao, Ionospheric disturbances during the total solar eclipse on 16 February 1980, *Proc. Indian Natl. Sci. Acad., Ser. A*, **48**, 406, 1982.
- Balan, N., B. Jayachandran, R. Balachandran Nair, S. P. Namboothiri, G. J. Bailey, and P. B. Rao, HF Doppler observations of vector plasma drifts in the evening *F* region at the magnetic equator, *J. Atmos. Terr. Phys.*, **54**, 1545, 1992.
- Bittencourt, J. A., and M. A. Abdu, A theoretical comparison between apparent and real vertical ionization drift velocities in the equatorial *F* region, *J. Geophys. Res.*, **86**, 2451, 1981.
- Booker, H. G., The role of acoustic gravity waves in the generation of spread *F* and ionospheric scintillation, *J. Atmos. Terr. Phys.*, **41**, 501, 1979.
- Booker, H. G., and H. W. Wells, Scattering of radio waves by the *F* region of the ionosphere, *J. Geophys. Res.*, **43**, 249, 1938.
- Cakir, S., G. Haerendel, and J. V. Eccles, Modeling the ionospheric response to artificially produced density enhancements, *J. Geophys. Res.*, **97**, 1193, 1992.
- Chiu, Y. T., and J. M. Straus, Rayleigh–Taylor and wind-driven instabilities of the nighttime equatorial ionosphere, *J. Geophys. Res.*, **84**, 3283, 1979.
- Farley, D. T., B. B. Balsley, R. F. Woodman, and J. P. McClure, Equatorial spread-*F*: Implications of VHF radar observations, *J. Geophys. Res.*, **75**, 7199, 1970.
- Fejer, B. G., and M. C. Kelley, Ionospheric irregularities, *Rev. Geophys. Space Phys.*, **18**, 401, 1980.
- Fejer, B. G., D. T. Farley, R. F. Woodman, and C. Calderon, Dependence of equatorial *F* region vertical drifts on season and solar cycle, *J. Geophys. Res.*, **84**, 5792, 1979.

- Hanson W. B., S. Sanatani, and T. N. L. Patterson, Influence of the E region dynamo on equatorial spread F , *J. Geophys. Res.*, **88**, 3169, 1983.
- Hanson, W. B., B. L. Cragin, and A. Dennis, The effects of vertical drift on the equatorial F region stability, *J. Atmos. Terr. Phys.*, **48**, 205, 1986.
- Hedin A. E., MSIS-86 thermospheric model, *J. Geophys. Res.*, **92**, 4649, 1987.
- Heelis, R. A., P. C. Kendall, R. J. Moffett, W. Windle, and H. Rishbeth, Electrical coupling of the E and F regions and its effects on F region drifts and winds, *Planet. Space Sci.*, **22**, 743, 1974.
- Hysell, D. L., M. C. Kelley, W. E. Swartz, and R. F. Woodman, Seeding and layering of equatorial spread F by gravity waves, *J. Geophys. Res.*, **95**, 17253, 1990.
- Jayachandran, B., N. Balan, S. P. Namboothiri, and P. B. Rao, HF Doppler observations of vertical plasma drifts in the evening F region at the equator, *J. Geophys. Res.*, **92**, 11253, 1987.
- Kelley, M. C., Equatorial spread F : Recent results and outstanding problems, *J. Atmos. Terr. Phys.*, **47**, 745, 1985.
- Kelley, M. C., and D. L. Hysell, Equatorial spread F and neutral atmospheric turbulence: A review and a comparative anatomy, *J. Atmos. Terr. Phys.*, **53**, 695, 1991.
- Maruyama, T., A diagnostic model for equatorial spread F , 1, Model description and application to electric field and neutral wind effects, *J. Geophys. Res.*, **93**, 14611, 1988.
- McFarland, M., D. L. Albritton, F. C. Fehsenfeld, E. E. Ferguson, and A. F. Schmeltekopf, Flow-drift technique for ion mobility and ion-molecule reaction rate constant measurements, 2, Positive ion reaction of N^+ , O^+ and N_2^+ with O_2 and O^+ with N_2 from thermal to ~ 2 eV, *J. Chem. Phys.*, **59**, 6620, 1973.
- Mendillo, M., J. Baumgardner, X. Pi, P. J. Sultan, and R. T. Tsunoda, Onset conditions for equatorial spread F , *J. Geophys. Res.*, **97**, 13865, 1992.
- Ossakow, S. L., Spread F theories - A review, *J. Atmos. Terr. Phys.*, **43**, 437, 1981.
- Ossakow, S. L., S. T. Zalesak, B. E. McDonald, and P. K. Chaturvedi, Nonlinear equatorial spread F : Dependence on altitude of the F peak and bottomside background electron density gradient scale height, *J. Geophys. Res.*, **84**, 17, 1979.
- Raghavarao, R., S. P. Gupta, R. Sekar, R. Narayanan, J. N. Desai, R. Sridharan, V. V. Basu, and V. Sudhakar, In-situ measurements of winds, electric fields and electron densities at the onset of equatorial spread F , *J. Atmos. Terr. Phys.*, **49**, 485, 1987.
- Rastogi, R. G., Seasonal and solar cycle variations of equatorial spread F in the American zone, *J. Atmos. Terr. Phys.*, **42**, 593, 1980.
- Rishbeth, H., Polarization fields produced by winds in the equatorial F region, *Planet. Space Sci.*, **19**, 357, 1971.
- Sastri, J. H., Duration of equatorial spread F , *Ann. Geophys.*, **2**, 353, 1984.
- Sastri, J. H., and B. S. Murthy, Spread F at Kodaikanal, *Ann. Geophys.*, **2**, 285, 1975.
- Scannapieco, A. J., and S. L. Ossakow, Nonlinear equatorial spread F , *Geophys. Res. Lett.*, **3**, 451, 1976.
- Somayajulu, V. V., B. V. Krishna Murthy, and K. S. V. Subbarao, Response of nighttime equatorial F region to magnetic disturbances, *J. Atmos. Terr. Phys.*, **53**, 965, 1991.
- Strobel, D. F., and M. B. McElroy, The F_2 -layer at mid-latitudes, *Planet. Space Sci.*, **18**, 1181, 1970.
- Tsunoda, R. T., Time evolution and dynamics of equatorial backscatter plumes, 1, Growth phase, *J. Geophys. Res.*, **86**, 139, 1981.
- Tsunoda, R. T., Control of the seasonal and longitudinal occurrence of equatorial scintillations by the longitudinal gradient in integrated E region Pedersen conductivity, *J. Geophys. Res.*, **90**, 447, 1985.
- Vyas, G. D., and H. Chandra, Ionospheric zonal drift reversal and equatorial spread F , *Ann. Geophys.*, **9**, 299, 1991.
- Woodman, R. F., and C. La Hoz, Radar observations of F region equatorial irregularities, *J. Geophys. Res.*, **81**, 5447, 1976.

G. J. Bailey and N. Balan, Department of Applied and Computational Mathematics, University of Sheffield, Sheffield S10 2TN, England.

B. Jayachandran, Department of Physics, University of Kerala, Trivandrum 695 581, India.

P. B. Rao, National MST Radar Center, Tirupati 517 502, India.

J. H. Sastri, Indian Institute of Astrophysics, Bangalore 560 034, India.

(Received July 8, 1992;
revised January 4, 1993;
accepted January 26, 1993.)